Controllable Growth and Transfer of Monolayer MoS_2 on Au Foils and Its Potential Application in Hydrogen Evolution Reaction

Jianping Shi,[†,‡,⊥] Donglin Ma,[‡,⊥] Gao-Feng Han,[§] Yu Zhang,[†,‡] Qingqing Ji,[‡] Teng Gao,[‡] Jingyu Sun,[‡] Xiuju Song,[‡] Cong Li,[†,‡] Yanshuo Zhang,[†,‡] Xing-You Lang,[*,§] Yanfeng Zhang,[*,†,‡] and Zhongfan Liu[‡]

[†]Department of Materials Science and Engineering, College of Engineering, Peking University, Beijing 100871, People's Republic of China, [‡]Center for Nanochemistry (CNC), Beijing National Laboratory for Molecular Sciences, College of Chemistry and Molecular Engineering, Peking University, Beijing 100871, People's Republic of China, and [§]Key Laboratory of Automobile Materials (Jilin University), Ministry of Education, School of Materials Science and Engineering, Jilin University, Changchun 130022, People's Republic of China. [⊥]These authors contributed equally.

ABSTRACT Controllable synthesis of monolayer MoS_2 is essential for fulfilling the application potentials of MoS_2 in optoelectronics and valleytronics, *etc.* Herein, we report the scalable growth of high quality, domain size tunable (edge length from ~200 nm to 50 μm), strictly monolayer MoS_2 flakes or even complete films on commercially available Au foils, *via* low pressure chemical vapor deposition method. The as-grown MoS_2 samples can be transferred onto arbitrary substrates like SiO_2/Si and quartz with a perfect preservation of the crystal quality, thus probably facilitating its versatile applications. Of particular interest, the nanosized triangular MoS_2 flakes on Au foils are proven to be excellent electrocatalysts for hydrogen evolution reaction, featured by a rather low Tafel slope (61 mV/decade) and a relative high exchange current density (38.1 μA/cm^2). The excellent electron coupling between MoS_2 and Au foils is considered to account for the extraordinary hydrogen evolution reaction activity. Our work reports the synthesis of monolayer MoS_2 when introducing metal foils as substrates, and presents sound proof that monolayer MoS_2 assembled on a well selected electrode can manifest a hydrogen evolution reaction property comparable with that of nanoparticles or few-layer MoS_2 electrocatalysts.

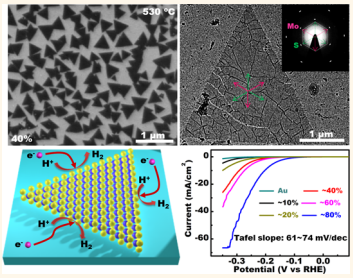

KEYWORDS: molybdenum disulfide · chemical vapor deposition · thickness control · hydrogen evolution reaction · Au foil

The significance of two-dimensional (2D) atomic layer thin materials has been fully demonstrated by a series of fascinating performances emerged in graphene.[1,2] However, the zero band gap property of graphene impedes its applications in carbon-based nanoelectronics and optoelectronics.[3] In this regard, transition metal dichalcogenides (TMDCs) with lamellar structures have subsequently drawn great interest due to its sizable band gap with indirect to direct tunability from bulk to monolayer,[4−6] and plenty of intriguing performances in electrical,[7] optical,[8] and photovoltaic devices.[9]

Synthesizing uniform monolayer TMDCs films with high crystal quality and large domain size should be the premise to fulfill the application potentials of TMDCs, and a variety of synthesis methods have been developed so far. Top-down micromechanical exfoliation[10,11] and ionic intercalation[12] are first employed to produce atomically thin TMDCs films, the production of which is nevertheless of nonuniform thickness and versatile size distributions, and in particular incompatible with efficient batch fabrication. Recently, several bottom-up methods, such as transition metal sulfurization,[13] decomposition of thiomolybdates,[14] and physical vapor deposition,[15] have been explored to synthesize of TMDCs films on insulating substrates, but still resulting in uncontrollable film thickness ranging from monolayer to few-layer. Compared with above-mentioned routes, chemical vapor deposition (CVD) technique is more simple and efficient in synthesizing monolayer TMDCs films[16−21] because of its wide tunability in growth parameters and substrates.[22] Note that the CVD TMDCs films grown on insulating substrates (SiO_2,[23]

* Address correspondence to yanfengzhang@pku.edu.cn, xylang@jlu.edu.cn.

Received for review June 13, 2014 and accepted September 11, 2014.

Published online September 11, 2014
10.1021/nn503211t

mica,[24] and sapphire[25]) have demonstrated their perfect application potentials in electronic and photovoltaic devices.

In particular, theoretical calculations have indicated that the free energy of hydrogen bonding to the Mo-terminated edge of MoS_2 (a member of TMDCs) is close to that of Pt,[26] which makes MoS_2 a potentially low-cost, high-abundance substitute of Pt in electrocatalytic hydrogen evolution reaction (HER).[27−31] To this end, MoS_2-based HER electrocatalysts such as amorphous particles,[32] chemically exfoliated nanosheets,[33−35] mesopores,[36] as well as thin films[37,38] have been intensively synthesized in various routes. Although rather high HER activities have been obtained, the HER mechanism is still inconclusive due to the complexity of the reaction, probably mediated by a wide distribution of particle size and layers thickness, and the multiple surface texture, *etc.* Consequently, seeking for ideal systems, *e.g.*, 2D monolayer MoS_2 nanoislands with tunable sizes, would be helpful in establishing a direct correlation between the catalytic activity and the microscopic structure (namely the amount of edge sites), considering that the HER activity originates from the edges of MoS_2 while the basal planes are catalytically inert.[26,36,39] It is worthy of mention that ultrahigh vacuum (UHV) deposition and recognition of MoS_2 nanoislands was realized on Au(111) by scanning tunneling microscope (STM).[40] The as-grown sample presented a rather low Tafel slope of ∼55−60 mV/decade and rather high HER activity. However, the fabrication process involved in obtaining MoS_2/Au(111) was nevertheless instrument-dependent and cost-ineffective, hence retarding the large-scale production and the practical application of monolayer MoS_2 in HER.

Herein, we demonstrate, for the first time, the scalable synthesis of monolayer MoS_2 on commercially available Au foils *via* a facile low-pressure CVD (LPCVD) method. Notably, the edge length of the triangular monolayer MoS_2 flake is found to be tunable from nanometer to micrometer by varying the growth temperature or the precursor substrate distance. The domain size, crystal quality, thickness, and uniformity of as-synthesized MoS_2 on Au foils and after transfer were probed by various characterization techniques. Moreover, the HER performance of as-grown nanosized monolayer MoS_2 on Au foils was examined as a function of the edge density. The mechanism for the enhanced HER activity was investigated.

RESULTS AND DISCUSSION

Figure 1a schematically illustrates the formation of MoS_2 2D flakes on Au foils, where the precursor upstream MoO_3 powder was partially reduced by vaporized S to form volatile suboxide species of MoO_{3-x}, and then sulfurized into MoS_2 on the downstream Au foils with the aid of Ar carrier gas, as described by the reaction:

$$S_2 + MoO_{3-x} \rightarrow MoS_2 + SO_2 \quad (1)$$

The LPCVD setup employed in this work is depicted in Figure 1b (see Methods for further details of the growth methodology). The X-ray photoemission spectroscopy (XPS) spectra (Figure 1c and Supporting Information Figure S1) was first captured to confirm the formation of MoS_2, as characterized by the Mo $3d_{5/2}$ (at 229.1 eV) and Mo $3d_{3/2}$ (at 232.3 eV) peaks associated with Mo^{4+}, as well as the S $2p_{3/2}$ (at 162.1 eV) and S $2p_{1/2}$ (at 163.2 eV) peaks assigned to S^{2-}, which are all in good agreement with those previously reported for MoS_2.[16]

Scanning electron microscope (SEM) (Figure 1d−g) micrographs were then captured to show the domain size evolution of as-grown MoS_2 on Au foils. Notably, after 1 h growth at 530 °C (Figure 1d), triangular MoS_2 flakes with nearly uniform edge lengths of ∼200 nm can be obtained on Au foils. Upon increasing the growth temperature to 680 °C while keeping other growth parameters identical (Figure 1e and Supporting Information Figure S2), the edge length of triangular MoS_2 flake can be enlarged to ∼55 μm. Further increasing the growth temperature to ∼750 °C leads to a decline in edge length (∼30 μm) of the triangular domains (Figure 1g). This is because, at higher temperature, the adsorption amount of sulfurized precursors on Au foils should be dramatically decreased, leading to a decreased growth rate of MoS_2. From Figure 1f,g, some particles which arise from the incomplete sulfuration of suboxide species (MoO_{3-x}) are sometimes observed either on Au substrates or on MoS_2 flakes. Intriguingly, due to their large domain sizes, the 2D MoS_2 flakes (formed at 680 °C) can be visible by optical microscope (OM) (Figure 1h). Otherwise, it is worthy of mention that, with the LPCVD method, the size of as-grown MoS_2 sample is limited both by the size of Au foils and the dimension for the uniform deposition of sulfurized precursor. The photograph in Figure 1i represents a MoS_2 example of 3 × 3 cm^2 in size.

Raman spectroscopy measurements were then carried out to probe the layer thickness as well as the crystal quality of the as-grown MoS_2 samples on Au foils (Figure 1j). Two typical Raman peaks corresponding to the out-of-plane vibration of S atoms (A_{1g}) at ∼406.9 cm^{-1} and in-plane vibration of Mo and S atoms (E^1_{2g}) at ∼387.0 cm^{-1} can be obtained to be invariable with the growth temperature. Especially, the frequency difference $\Delta \sim 19.9$ cm^{-1} acquired from the various samples shown in Figure 1d−g seems in good agreement with that reported for monolayer MoS_2,[41] thus indicating tentatively monolayer MoS_2 formation on Au foils regardless of the synthesis temperatures. The growth of MoS_2 on Au foils is thus considered to obey a two-dimensional feature.

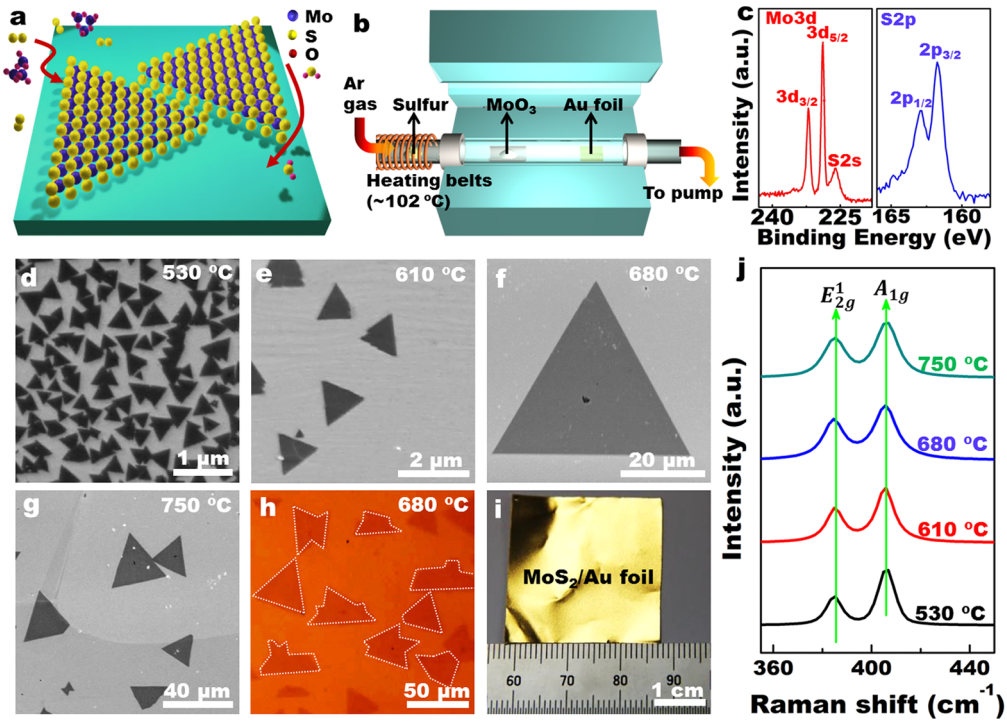

Figure 1. LPCVD synthesis of monolayer MoS_2 on Au foils. (a) Schematic view of the surface growth of MoS_2 on Au foils. (b) Experimental setup of the LPCVD system. (c) XPS spectra of as-grown MoS_2 on Au foils. (d–g) SEM images of MoS_2 triangular flakes grown under distinct growth temperatures displaying different domain sizes, respectively. (h) OM image of as-grown MoS_2 flakes on Au foils with more complicated shapes. (i) Photograph of the batch production feature of MoS_2 on Au foils. (j) Raman spectra of MoS_2 flakes shown in (d–g) indicating the monolayer nature.

It is expected that, in the sample growth zone, the concentration of MoO_{3-x} will decrease with increasing the distance between MoO_3 precursor and Au substrate (D_{ss}), leading to different coverage of MoS_2 on the substrate. To confirm this, a series of Au foils were successively placed on the downstream region of the quartz tube (Figure 2a). It is intriguing to find that, with the different D_{ss} (10.0, 11.0, and 12.0 cm) (corresponding to Figure 2b–d, ~ 530 °C growth), the coverage of MoS_2 on Au foils can be effectively tuned from ~70%, 50%, to 10%, as clearly imaged by SEM with the edge lengths of the triangular flakes variable from ~500 to ~200 nm. Similarly, upon increasing the growth temperature to 680 °C, MoS_2 samples with coverage of ~90%, 80%, and 10% can also be obtained with the edge lengths of the flakes tunable from ~50 to 20 μm (Figure 2e-g, ~ 680 °C growth). In this regard, through an appropriate control of D_{ss} and the growth temperature, near complete monolayer MoS_2 films can be obtained directly on Au foils *via* a facile LPCVD method (see Supporting Information Figure S3). Moreover, it is urgent to know if the MoS_2 flakes with different D_{ss} (or diverse coverage) are all of the same thickness. Raman measurements performed on the samples (Figure 2e,i) show nearly the same frequency difference $\Delta \sim 19.9$ cm^{-1} for the two typical vibrational modes of A_{1g} and E^1_{2g}, suggestive of the uniform monolayer nature.[41] The uniform monolayer growth regardless of growth temperature and source-substrate distance (D_{ss}) strongly suggests the 2D growth feature of MoS_2 on Au foils, which is probably mediated by the relative strong interaction between MoS_2 and Au foils. This is in sharp contrast with that of MoS_2 on insulating SiO_2, sapphire *etc.*, with the probability of forming few-layer. Considering its batch production nature, tunable coverage, and strict monolayer thickness, MoS_2 grown on Au foils may serve as a potential candidate in diverse fields such as effective photocatalysts,[42] solar energy funnels,[43] and integrated circuits.[44]

Transference of the as-grown LPCVD MoS_2 samples onto arbitrary substrates like SiO_2/Si and quartz is highly demanded for revealing the film thickness, the intrinsic electronic and optical properties, as well as for engineering its wide applications. Herein, a chemical wet etching method is utilized to transfer the as-grown samples, and the transferability in large scales is displayed in Figure 3a showing the photographs of MoS_2 films on SiO_2/Si and quartz substrates, where a light yellow color can be noticed on the substrates. In microscopic scales, the MoS_2 triangular flakes, after being transferred onto SiO_2/Si and quartz (Figure 3b,c and Supporting Information Figure S4) and imaged by OM, present perfect preservation of the flake shapes, suggestive of a near intact transfer process. Notably, the near complete monolayer MoS_2 film is also transferable, as evidenced by the near uniform purple contrast on SiO_2/Si in contrast with the earthy yellow substrate (Figure 3d).

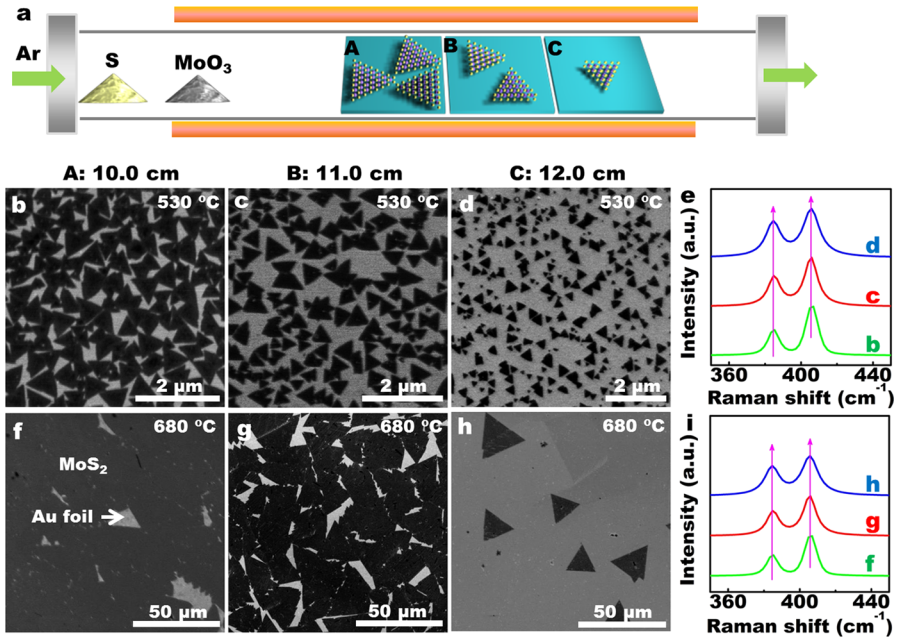

Figure 2. SEM images of monolayer MoS_2 grown on Au foils with different precursor substrate distance (D_{ss}) and different temperature. (a) A schematic illustration of the coverage or flake size dependence on D_{ss}. (b–d) SEM images of monolayer MoS_2 samples with coverage of ~70%, 50%, and 10% synthesized at the same condition (grown at 530 °C) but with different D_{ss} of ~10.0, 11.0, and 12.0 cm, respectively. (e) Raman spectra of the monolayer MoS_2 flakes shown in (b–d). (f–h) Corresponding SEM images of MoS_2 growth at 680 °C with coverage of ~90%, 80%, and 10%, respectively. (i) Raman spectra of MoS_2 flakes shown in (f–h).

To reveal the film thickness, atomic force microscopy (AFM) was then employed to characterize the transferred MoS_2 flake on the relative flat SiO_2/Si substrate. An apparent height of ~0.9 nm is observed from the AFM section-view analysis across the flake edge in Figure 3e, which provides more straightforward proof of its monolayer nature (Figure 3f).[17] Notably, a number of wrinkles, usually possessing a height of >1 nm, can be noticed which is probably generated either from the transfer process, or from the as-grown state due to the different thermal expansion coefficients of the MoS_2 and Au foil (7.0×10^{-6} K^{-1} and 14.2×10^{-6} K^{-1} for monolayer MoS_2 and Au foils, respectively, at 300 K).[45]

In a further step, it is also critical to know the crystallinity of the transferred monolayer MoS_2 flakes. To this end, the as-grown MoS_2 flake on Au foils was subsequently transferred onto a carbon film supported on copper grids for transmission electron microscopy (TEM) characterization. Figure 3g presents the bright-field TEM (BF-TEM) image of a triangular MoS_2 flake, on which some dark contrast lines are noticed to be in parallel with the MoS_2 wrinkles as observed from AFM images. Corresponding selective area electron diffraction (SAED) pattern shows only one set of hexagonally arranged diffraction spots, strongly suggestive of the single-crystal nature of the MoS_2 triangle (Figure 3h). Otherwise, the intensity line profile captured along the four diffraction spots (circled in the dashed square) (Figure 3h) reveals that the diffraction spots can be divided into two families with k_a spots associated with Mo sublattice, and k_b spots point toward the S sublattice.

Notably, the intensity of the k_a spots seems a little bit higher (~15% for an 200 kV electron beam) than that of k_b (inset of Figure 3h), which suggests the Mo-terminated feature of the flake edge (as indicated by the arrows in Figure 3g,h) by referring to the similar TEM result for the triangular MoS_2 flakes grown on SiO_2 and related theoretical calculations.[23] Of particular importance, the high resolution TEM (HRTEM) image (Figure 3i) focused on the folded film edge usually presents a single black line contrast, providing complementary proof of the monolayer nature of the MoS_2 flake. In addition to single-crystal triangles, more complicated shapes, *e.g.*, stars or butterfly like shapes (Supporting Information Figure S5) may also appear which can be regarded as aggregates of triangular flakes. Figure 3j,k exhibits the BF-TEM image and diffraction pattern of a polygonal MoS_2 flake with 20° orientation difference. Figure 3l shows the corresponding color-coded dark-field TEM image constructed by overlaying different colors reveal different lattice orientations as deduced from the corresponding SAED pattern (Figure 3k). Bright-field and dark-filed TEM images, and corresponding SAED pattern of this polygonal flake, are shown in Supporting Information Figure S6.

Raman mapping was employed to probe the thickness uniformity and the crystal quality of as-grown monolayer MoS_2 flakes (Figure 4a). Both triangular, hexagonal, butterfly like individual flakes, and nearly complete MoS_2 films present rather homogeneous

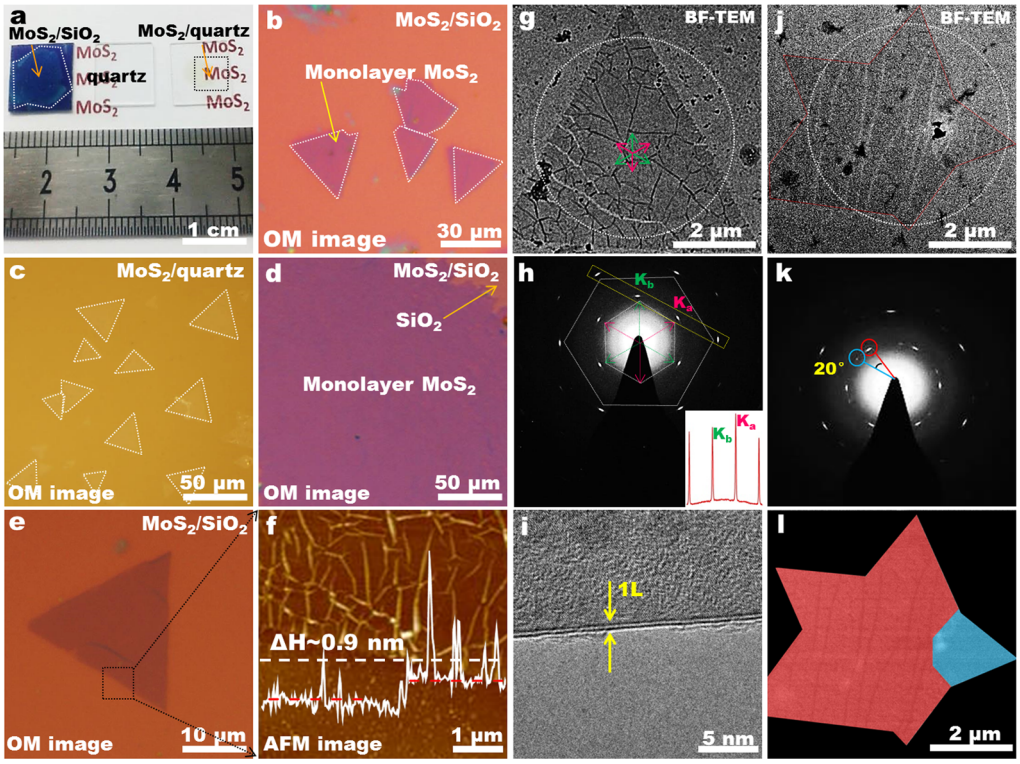

Figure 3. Transferability of the uniform monolayer MoS_2 onto arbitrary substrates of SiO_2/Si and quartz. (a) Photographs of monolayer MoS_2 films on SiO_2/Si, a bare quartz substrate, and MoS_2 on quartz. (b and c) Optical images of submonolayer MoS_2 flakes after transference onto SiO_2/Si and quartz substrates. (d) Optical image of a complete monolayer MoS_2 film after transference onto SiO_2/Si. (e) A triangular MoS_2 flake transferred onto SiO_2/Si substrate. (f) Atomic force microscopy (AFM) image captured from the dashed box in (e) and corresponding section-view along the dashed arrow showing the monolayer feature of the flake (~0.9 nm in apparent height). (g) TEM image of a MoS_2 triangle transferred on a carbon film supported on copper grids. (h) SAED pattern from (g) (selected area marked by the circle) with the inset showing a line profile of the diffraction spots marked by a rectangle. (i) TEM image on a folded edge indicating the monolayer nature of the MoS_2 flake. (j) Bright-field TEM image of a polygonal MoS_2 flake. (k) Corresponding SAED patterns from (j) (selected area marked by the circle). (l) Color-coded overlay of dark-field TEM image corresponding with the two red- and blue-circled spots in (k).

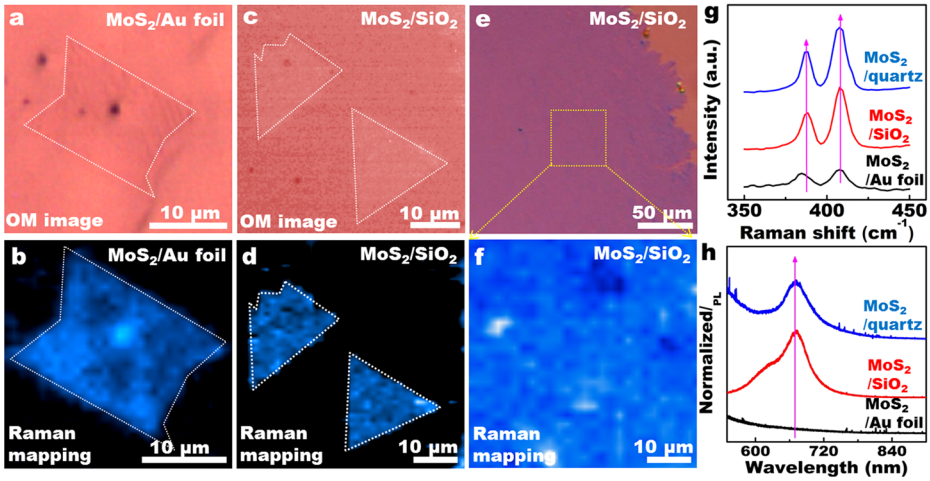

Figure 4. Raman and photoluminescence (PL) spectra of monolayer MoS_2 flakes and complete monolayer films prior to (on Au foils) and after transference onto standard SiO_2/Si substrates (300 nm thick). (a–f) OM and Raman mapping images of a butterfly like shape MoS_2 flake on Au foils, near triangular MoS_2 flakes transferred onto SiO_2/Si, and complete MoS_2 films on SiO_2/Si with the Raman signal integrated from 350 to 450 cm^{-1}, respectively. (g and h) Single point Raman and PL spectra of as-grown MoS_2 on Au, transferred MoS_2 on SiO_2, and on quartz, respectively, with PL intensity normalized by Raman A_{1g} phonon peak at ~406.9 cm^{-1}.

contrasts in the Raman mapping micrographs (Figure 4b, also see Supporting Information Figures S7 and S8), providing tentative spectroscopy proof of the rather high thickness uniformity of as-grown MoS_2 samples. More single point Raman spectra selected randomly from a 20 μm × 20 μm mapping area

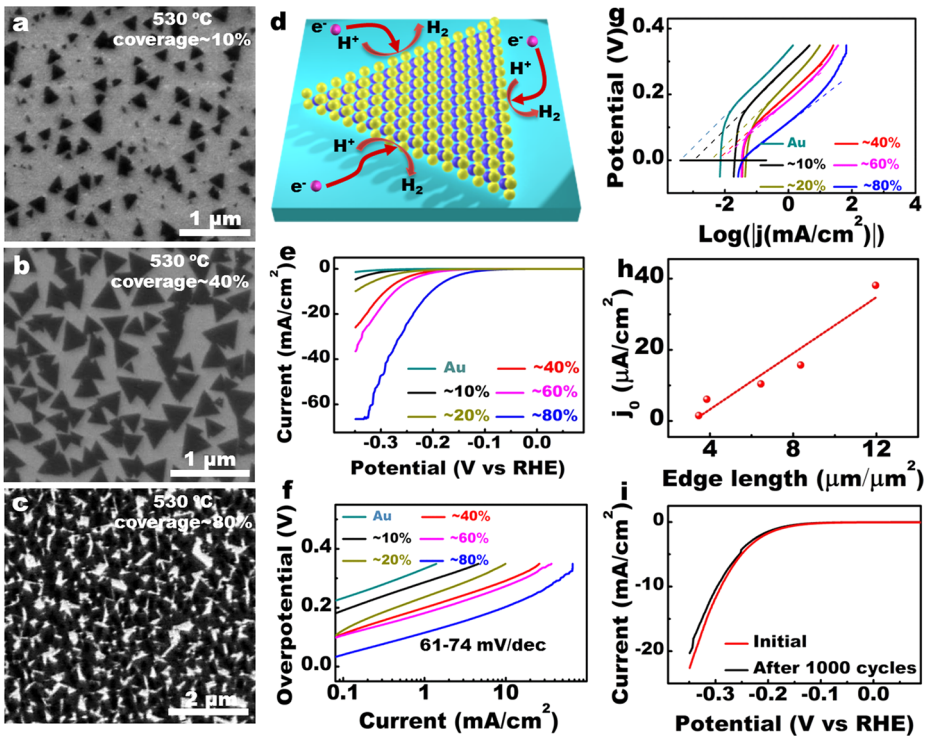

Figure 5. HER activity of nanosized as-grown MoS_2 on Au foils. (a–c) SEM images of monolayer MoS_2 flakes with different coverage (10%, 40%, and 80%, respectively). (d) Schematic view illustrating the edges of monolayer MoS_2 functioning as the active catalytic sites for HER. (e and f) Coverage-dependent polarization curves and corresponding Tafel plots of as-grown monolayer MoS_2 on Au foils samples. (g) Calculated exchange current densities of different samples by applying an extrapolation method to the Tafel plots. (h) Statistical relation of exchange current density with the edge length of MoS_2. (i) Durability test for the MoS_2/Au hybrid catalyst.

(Supporting Information Figures S7 and S8) again confirm the high thickness uniformity, since almost no shift of the typical vibrations modes (A_{1g}, E^1_{2g}) among different locations can be noticed, consistent with that of the published results for monolayer MoS_2.[46] In contrast, the OM views and Raman mapping images of MoS_2 flakes and even monolayers transferred onto SiO_2/Si are also captured in Figure 4c,d, and Figure 4e,f, respectively. The rather uniform Raman signals for the transferred samples provide more visual proof of the perfect thickness uniformity of the monolayer MoS_2 film.

A careful comparison of the Raman and photoluminescence (PL) spectra of MoS_2 prior to and after transfer was then carried out to show the different interface interactions, as well as the intrinsic electronic property of MoS_2. It is interesting to see that Raman spectra for the transferred samples on SiO_2 and on quartz (Figure 4g) present a similar frequency difference of $\Delta \sim 18.6\ cm^{-1}$ between E^1_{2g} and A_{1g} modes, a little bit smaller than that before transfer of $\Delta \sim 19.9\ cm^{-1}$. This phenomenon have been reported in recent works, in which a strong interface interaction was considered to enable a suppression of the in-plane vibration of Mo and S atoms (related to E^1_{2g} mode) due to a higher force constant.[47,48] For the transferred samples, the E^1_{2g} is red-shifted while with the A_{1g} remains unchanged, leading to a smaller Δ than that before transfer. Otherwise, the red-shift of the A_{1g} mode after transfer may also occur to be due to the relaxation of the strain effect, which arises from the conformation of MoS_2 overlayer to the substrate.[49] Meanwhile, the elimination of the charge transfer from Au to MoS_2 (n-doping effect) after sample transfer may also induce a blue-shift of the A_{1g} mode.[50,51] These two effects should work together to lead to no obvious change of A_{1g} mode. Consequently, the strain and the substrate doping effect should concurrently affect the Raman shift.

As mentioned earlier, PL spectra of the as-grown MoS_2 sample shows almost no feature at the wavelength range from 500 to 800 nm, probably due to a fluorescence quenching effect from Au foil substrates. However, after transfer onto SiO_2/Si and quartz, striking PL peaks appear at ~665.1 nm (1.864 eV) for MoS_2 on SiO_2 and 666.5 nm (1.860 eV) for MoS_2 on quartz (Figure 4h), with the peak positions in good agreement with the theoretical value for monolayer MoS_2.[52] This occurrence of typical PL single implies not only the high crystal quality of the transferred sample, but also the relaxation of the strong interface interaction between MoS_2 and Au.

The LPCVD monolayer MoS_2 on Au foils was then considered to be a probable system for exploring the electrocatalytic HER activity. A series of 530 °C grown MoS_2 samples with coverage from 10%, 40% to 80% (obtained in the same growth batch by only

adjusting D_{ss}) were selected to serves as electrocatalysts. The representative SEM images of the triangular MoS_2 samples are sequentially presented in Figure 5a–c, showing average edge length of 0.20 ± 0.04, 0.43 ± 0.03, and 0.49 ± 0.05 μm with increasing flake coverage, respectively. The HER process of MoS_2 as-grown on Au foils is schematically shown in Figure 5d, based on theoretical[26] and experimental results[30] that the HER activity relates closely to the edge sites ofMoS_2 flakes and the basal surfaces are catalytically inert. As presented by TEM data in Figure 3h, the edge of CVD grown triangular monolayer MoS_2 flake is predominantly Mo-terminated, which is reactive for HER.[53]

The HER activities of as-grown MoS_2 on Au foils with different flake sizes (or flake coverage) are reflected in the polarization curves in Figure 5e, with the Au foil serving as the reference. Clearly, all of the MoS_2/Au catalysts possess much lower onset overpotentials (η) than the Au foil, and the 80% coverage sample exhibits the lowest value of ~100 mV. Notably, this sample again presents an extremely large cathodic current density of ~50.5 mA/cm^2 at η = 300 mV, which is almost 25 times larger than that observed in bulk MoS_2[35] and much larger compared to the other four coverage samples in this work (15.3, 10.1, 5.7, and 3.9 mA/cm^2 corresponding to 60%, 40%, 20%, and 10%, respectively, at η = 300 mV).

The overall Tafel slopes were measured to be variable from 61 to 74 mV/decade (Figure 5f), with the lowest Tafel slope (61 mV/decade) achieved from the sample with ~80% coverage. This result is comparable with that of UHV deposited MoS_2/Au(111) of 55–60 mV/decade,[40] while it is much lower than that of CVD grown few-layer MoS_2 on glassy carbon (GC) electrodes (140–145 mV/decade).[37] As it is known, Tafel slope is an inherent property of the catalyst which is determined by the rate-limiting step of the HER.[54] Three possible principle steps have been proposed for the HER in acidic medium. The first is a primary discharge step (Volmer reaction, eq 2):

$$H_3O^+ + e^- \rightarrow H_{ads} + H_2O \quad (2)$$

which is followed by either the electrochemical desorption step (Heyrovsky reaction, eq 3) or recombination step (Tafel reaction, eq 4):

$$H_{ads} + H_3O^+ + e^- \rightarrow H_2 + H_2O \quad (3)$$

$$H_{ads} + H_{ads} \rightarrow H_2 \quad (4)$$

Under a specific set of conditions, once the Volmer reaction accounts for the rate-limiting step, a Tafel slope of ~120 mV/decade should result. In addition, Tafel slope of 30 or 40 mV/decade is associated with the Heyrovsky or Tafel reaction acting as the rate-limiting step, respectively. The Tafel slope of 61 mV/decade obtained in this work is close to that of MoS_2 nanoislands prepared in UHV,[40] suggesting the similar surface chemistry of as-grown monolayer MoS_2 on Au foils.

By applying extrapolation method to the Tafel plots, exchange current density (j_0), another parameter for the HER rate, can be deduced for all the samples (Figure 5a–c), where the sample with 80% coverage exhibits a remarkable j_0 of 38.1 μA/cm^2, which is by far the highest value among those reported for MoS_2 catalysts. Statistical relations of j_0 as a function of edge length per area of MoS_2 flakes on Au foils are also achieved in Figure 5h (see Supporting Information Table S1 for details). Intriguingly, the j_0 is correlated linearly with the edge length per area of MoS_2, accounting for a linear increase of HER activity with the growing number of the edge sites. Another important criterion for a good electrocatalyst lies in its high durability. Figure 5i shows the polarization curve of a 40% coverage sample, where negligible difference can be noticed between the initial and after 1000 cyclic voltammetry (CV) cycling states, indicative of the excellent electrocatalytic durability of LPCVD grown MoS_2 on Au foils.

This study hereby addresses that the as-grown coverage, or domain size tunable monolayer MoS_2 flakes on Au foils synthesized at 530 °C are potential systems for examining the HER performance and the potential mechanism of monolayer MoS_2. The strong electron coupling between MoS_2 and Au foil is explain the advanced HER activity, as proved by a rather low charge-transfer resistance (Supporting Information Table S1 and Figure S9). Meanwhile, it is worth mentioning that the polarization curves and corresponding Tafel plots of the samples synthesized at elevated growth temperatures (610, 680, and 750 °C) usually present retarded HER activities (Supporting Information Figure S10), probably due to the gradual reduction of the density of the active sites located at the edge of MoS_2 (Supporting Information Figure S11 and Table S2).

CONCLUSION

In summary, we have demonstrated for the first time the scalable synthesis of monolayer MoS_2 on commercially available Au foils *via* a facile LPCVD route. The high crystal quality, strict monolayer, tunable domain size, and transferrable MoS_2 samples should meet with the versatile applications in optoelectronic and electrocatalysis. As a special sample, the nanosized triangular MoS_2 flakes synthesized at a low growth temperature were demonstrated to be potential electrocatalysts for HER. A rather low Tafel slope (61 mV/decade) and a relative high exchange current density of ~38.1 μA/cm^2 were achieved, where the excellent electron coupling between MoS_2 and Au foils is proposed to account for the extraordinary HER activity. In brief, our work not only paves a new way

for the controllable growth of high quality, uniform monolayer MoS_2 by introducing Au foils as substrates, but also offers special insight for its versatile applications.

METHODS

MoS_2 Growth and Transfer. The growth of monolayer MoS_2 on Au foils was performed inside a multitemperature-zone tubular furnace (Lindberg/Blue M) equipped with a 1-in.-diameter quartz tube. Sulfur powder, placed outside the hot zone, was mildly sublimated at ~102 °C with heating belts, and carried by Ar gas (50 standard cubic centimeter per minute (sccm)), to the downstream growth zone. MoO_3 powders (Alfa Aesar, purity 99.9%) and Au foils (Alfa Aesar, purity 99.985%, thickness ~25 μm) were successively placed on the downstream region of the quartz tube. The MoO_3 powders were heated from room temperature to ~530 °C within 30 min along with a heating rate of ~17 °C/min. The pressure for growth MoS_2 on Au foils was set at 30 Pa, and the growth time was set at 60 min under growth temperatures of 530, 610, 680, and 750 °C, respectively. To transfer the as-grown MoS_2 films, the MoS_2/Au sample was first spin coated with poly(methyl methacrylate) (PMMA) and then baked at 170 °C for 10 min. The sample was then soaked in Au etchant (tape TFA) for the removal of Au. Finally, the PMMA-supported MoS_2 was rinsed with deionized (DI) water and a fresh SiO_2/Si substrate or other substrates were then used to "fish out" the PMMA-capped MoS_2 film, followed by rinsing with acetone for removing the PMMA.

Characterizations of MoS_2 Films. The prepared MoS_2 flakes were systematically characterized using optical microscopy (Olympus DX51), Raman spectroscopy (Horiba, LabRAM HR-800, excitation light ~514 nm), SEM (Hitachi S-4800, acceleration voltage of 1−5 kV), XPS (Kratos, Axis Ultra, Mg Kα as the excitation source), PL (Horiba, LabRAM HR-800, excitation light of 514 nm in wavelength), AFM (Vecco Nanoscope III), and TEM (JEOL JEM-2100 LaB6 for HRTEM; acceleration voltage of 200 kV. Tecnai T20 for DF-TEM; acceleration voltage of 200 kV).

Electrochemical Measurements. All of the electrochemical measurements were performed in a three-electrode system on an electrochemical workstation (CHI660D), using MoS_2 flakes on Au foils as the working electrode, a Pt foil as a counter electrode, and a saturated calomel reference electrode (SCE). All of the potentials were calibrated by a reversible hydrogen electrode (RHE). Linear sweep voltammetry with a scan rate of 5 mV/s, from +0.30 to −0.35 V *vs* RHE was conducted in 0.5 M H_2SO_4 (sparged with pure N_2, purity 99.999%). The Nyquist plots were obtained with frequencies ranging from 100 kHz to 0.1 Hz at an overpotential of 10 mV. The impedance data were fitted to a simplified Randles circuit to extract the series and charge-transfer resistances.

Conflict of Interest: The authors declare no competing financial interest.

Acknowledgment. This work was financially supported by National Natural Science Foundation of China (Grants Nos.51222201, 51290272, 51472008, 21201012, 51121091, 51072004, and 51201069) and the Ministry of Science and Technology of China (Grants Nos. 2011CB921903, 2012CB921404, 2012CB933404, 2013CB932603, and 2011CB933003), the Keygrant Project of Chinese Ministry of Education (Grants No. 313026) and the Program for New Century Excellent Talents in University (Grants No. NCET-10-0437).

Supporting Information Available: More Raman spectra, OM, SEM, XPS, and TEM images; and more polarization curves, Tafel plots, and nyquist plots of as-grown MoS_2 on Au foils or transferred on quartz and on a carbon film supported on copper grids. This material is available free of charge *via* the Internet at http://pubs.acs.org.

REFERENCES AND NOTES

1. Novoselov, K.; Geim, A. K.; Morozov, S.; Jiang, D.; Grigorieva, M. K. I.; Dubonos, S. V.; Firsov, A. Two-Dimensional Gas of Massless Dirac Fermions in Graphene. *Nature* **2005**, *438*, 197–200.
2. Berger, C.; Song, Z.; Li, X.; Wu, X.; Brown, N.; Naud, C.; Mayou, D.; Li, T.; Hass, J.; Marchenkov, A. N.; *et al.* Electronic Confinement and Coherence in Patterned Epitaxial Graphene. *Science* **2006**, *312*, 1191–1196.
3. Novoselov, K. Graphene: Mind the Gap. *Nat. Mater.* **2007**, *6*, 720–721.
4. Mak, K. F.; He, K.; Lee, C.; Lee, G. H.; Hone, J.; Heinz, T. F.; Shan, J. Tightly Bound Trions in Monolayer MoS_2. *Nat. Mater.* **2013**, *12*, 207–211.
5. Zhang, Y.; Chang, T.-R.; Zhou, B.; Cui, Y.-T.; Yan, H.; Liu, Z.; Schmitt, F.; Lee, J.; Moore, R.; Chen, Y.; *et al.* Direct Observation of the Transition from Indirect to Direct Bandgap in Atomically Thin Epitaxial $MoSe_2$. *Nat. Nanotechnol.* **2014**, *9*, 111–115.
6. Mak, K. F.; Lee, C.; Hone, J.; Shan, J.; Heinz, T. F. Atomically Thin MoS_2: A New Direct-Gap Semiconductor. *Phys. Rev. Lett.* **2010**, *105*, 136805.
7. Wu, S.; Ross, J. S.; Liu, G.-B.; Aivazian, G.; Jones, A.; Fei, Z.; Zhu, W.; Xiao, D.; Yao, W.; Cobden, D.; *et al.* Electrical Tuning of Valley Magnetic Moment through Symmetry Control in Bilayer MoS_2. *Nat. Phys.* **2013**, *9*, 149–153.
8. Mak, K. F.; He, K.; Shan, J.; Heinz, T. F. Control of Valley Polarization in Monolayer MoS_2 by Optical Helicity. *Nat. Nanotechnol.* **2012**, *7*, 494–498.
9. Wang, Q.; Kalantar-Zadeh, K.; Kis, A.; Coleman, J. N.; Strano, M. S. Electronics and Optoelectronics of Two-Dimensional Transition Metal Dichalcogenides. *Nat. Nanotechnol.* **2012**, *7*, 699–712.
10. Britnell, L.; Ribeiro, R.; Eckmann, A.; Jalil, R.; Belle, B.; Mishchenko, A.; Kim, Y.-J.; Gorbachev, R.; Georgiou, T.; Morozov, S.; *et al.* Strong Light-Matter Interactions in Heterostructures of Atomically Thin Films. *Science* **2013**, *340*, 1311–1314.
11. Li, H.; Wu, J.; Yin, Z.; Zhang, H. Preparation and Applications of Mechanically Exfoliated Single-Layer and Multilayer MoS_2 and WSe_2 Nanosheets. *Acc. Chem. Res.* **2014**, *47*, 1067–1075.
12. Coleman, J. N.; Lotya, M.; O'Neill, A.; Bergin, S. D.; King, P. J.; Khan, U.; Young, K.; Gaucher, A.; De, S.; Smith, R. J.; *et al.* Two-Dimensional Nanosheets Produced by Liquid Exfoliation of Layered Materials. *Science* **2011**, *331*, 568–571.
13. Shi, Y.; Zhou, W.; Lu, A.-Y.; Fang, W.; Lee, Y.-H.; Hsu, A. L.; Kim, S. M.; Kim, K. K.; Yang, H.; Li, L.-J.; *et al.* Van der Waals Epitaxy of MoS_2 Layers Using Graphene as Growth Templates. *Nano Lett.* **2012**, *12*, 2784–2791.
14. Liu, K.-K.; Zhang, W.; Lee, Y.-H.; Lin, Y.-C.; Chang, M.-T.; Su, C.-Y.; Chang, C.-S.; Li, H.; Shi, Y.; Zhang, H.; *et al.* Growth of Large-Area and Highly Crystalline MoS_2 Thin Layers on Insulating Substrates. *Nano Lett.* **2012**, *12*, 1538–1544.
15. Helveg, S.; Lauritsen, J. V.; Lægsgaard, E.; Stensgaard, I.; Nørskov, J. K.; Clausen, B. S.; Topsøe, H.; Besenbacher, F. Atomic-Scale Structure of Single-Layer MoS_2 Nanoclusters. *Phys. Rev. Lett.* **2000**, *84*, 951.
16. Wang, X.; Feng, H.; Wu, Y.; Jiao, L. Controlled Synthesis of Highly Crystalline MoS_2 Flakes by Chemical Vapor Deposition. *J. Am. Chem. Soc.* **2013**, *135*, 5304–5307.
17. Lee, Y.-H.; Zhang, X.-Q.; Zhang, W.; Chang, M.-T.; Lin, C.-T.; Chang, K.-D.; Yu, Y.-C.; Wang, J. T.-W.; Chang, C.-S.; Li, L.-J.; *et al.* Synthesis of Large-Area MoS_2 Atomic Layers with Chemical Vapor Deposition. *Adv. Mater.* **2012**, *24*, 2320–2325.
18. Ling, X.; Lee, Y.-H.; Lin, Y.; Fang, W.; Yu, L.; Dresselhaus, M. S.; Kong, J. Role of the Seeding Promoter in MoS_2 Growth by Chemical Vapor Deposition. *Nano Lett.* **2014**, *14*, 464–472.
19. Huang, J.-K.; Pu, J.; Hsu, C.-L.; Chiu, M.-H.; Juang, Z.-Y.; Chang, Y.-H.; Chang, W.-H.; Iwasa, Y.; Takenobu, T.; Li, L.-J. Large-Area Synthesis of Highly Crystalline WSe_2 Monolayers and Device Applications. *ACS Nano* **2014**, *8*, 923–930.

20. Lee, Y.-H.; Yu, L.; Wang, H.; Fang, W.; Ling, X.; Shi, Y.; Lin, C.-T.; Huang, J.-K.; Chang, M.-T.; Chang, C.-S.; *et al.* Synthesis and Transfer of Single-layer Transition Metal Disulfides on Diverse Surfaces. *Nano Lett.* **2013**, *13*, 1852–1857.
21. Zhang, W.; Huang, J.-K.; Chen, C.-H.; Chang, Y.-H.; Cheng, Y.-J.; Li, L.-J. High-Gain Phototransistors Based on A CVD MoS_2 Monolayer. *Adv. Mater.* **2013**, *25*, 3456–3461.
22. Najmaei, S.; Liu, Z.; Zhou, W.; Zou, X.; Shi, G.; Lei, S.; Yakobson, B. I.; Idrobo, J.-C.; Ajayan, P. M.; Lou, L. Vapour Phase Growth and Grain Boundary Structure of Molybdenum Disulphide Atomic Layers. *Nat. Mater.* **2013**, *12*, 754–759.
23. van der Zande, A. M.; Huang, P. Y.; Chenet, D. A.; Berkelbach, T. C.; You, Y.; Lee, G.-H.; Heinz, T. F.; Reichman, D. R.; Muller, D. A.; Hone, J. C. Grains and Grain Boundaries in Highly Crystalline Monolayer Molybdenum Disulphide. *Nat. Mater.* **2013**, *12*, 554–561.
24. Ji, Q.; Zhang, Y.; Gao, T.; Zhang, Y.; Ma, D.; Liu, M.; Chen, Y.; Qiao, X.; Tan, P.-H.; Kan, M.; *et al.* Epitaxial Monolayer MoS_2 on Mica with Novel Photoluminescence. *Nano Lett.* **2013**, *13*, 3870–3877.
25. Zhang, Y.; Zhang, Y.; Ji, Q.; Ju, J.; Yuan, H.; Shi, J.; Gao, T.; Ma, D.; Liu, M.; Chen, Y.; *et al.* Controlled Growth of High-Quality Monolayer WS_2 Layers on Sapphire and Imaging Its Grain Boundary. *ACS Nano* **2013**, *7*, 8963–8971.
26. Appel, A. M.; DuBois, D. L.; Rakowski DuBois, M. Molybdenum-Sulfur Dimers as Electrocatalysts for the Production of Hydrogen at Low Overpotentials. *J. Am. Chem. Soc.* **2005**, *127*, 12717–12726.
27. Voiry, D.; Yamaguchi, H.; Li, J.; Silva, R.; Alves, D. C.; Fujita, T.; Chen, M.; Asefa, T.; Shenoy, V. B.; Eda, G.; *et al.* Enhanced Catalytic Activity in Strained Chemically Exfoliated WS_2 Nanosheets for Hydrogen Evolution. *Nat. Mater.* **2013**, *12*, 850–855.
28. Wang, H.; Liu, Z.; Xu, S.; Kong, D.; Cha, J. J.; Zheng, G.; Hsu, P.-C.; Yan, K.; Bradsham, D.; Prinz, F. B.; *et al.* Electrochemical Tuning of Vertically Aligned MoS_2 Nanofilms and Its Application in Improving Hydrogen Evolution Reaction. *Proc. Natl. Acad. Sci. U.S.A.* **2013**, *110*, 19701–19706.
29. Xie, J.; Zhang, H.; Li, S.; Wang, R.; Sun, X.; Zhou, M.; Zhou, J.; Lou, X. W. D.; Xie, Y. Defect-Rich MoS_2 Ultrathin Nanosheets with Additional Active Edge Sites for Enhanced Electrocatalytic Hydrogen Evolution. *Adv. Mater.* **2013**, *25*, 5807–5813.
30. Bonde, J.; Moses, P. G.; Jaramillo, T. F.; Nørskov, J. K.; Chorkendorff, I. Hydrogen Evolution on Nano-Particulate Transition Metal Sulfides. *Faraday Discuss.* **2009**, *140*, 219–231.
31. Chhowalla, M.; Shin, S. H.; Ead, G.; Li, L.-J.; Loh, K. P.; Zhang, H. The Chemistry of Two-Dimensional Layered Transition Metal Dichalcogenide Nanosheets. *Nat. Chem.* **2013**, *5*, 263–275.
32. Li, Y.; Wang, H.; Xie, L.; Liang, Y.; Hong, G.; Dai, H. MoS_2 Nanoparticles Grown on Graphene: an Advanced Catalyst for the Hydrogen Evolution Reaction. *J. Am. Chem. Soc.* **2011**, *133*, 7296–7299.
33. Huang, X.; Zeng, Z.; Bao, S.; Wang, M.; Qi, X.; Fan, Z.; Zhang, H. Solution-Phase Epitaxial Growth of Noble Metal Nanostructures on Dispersible Single-Layer Molybdenum Disulfide Nanosheets. *Nat. Commun.* **2013**, *4*, 1444–1448.
34. Lukowski, M. A.; Daniel, A. S.; Meng, F.; Forticaux, A.; Li, L.; Jin, S. Enhanced Hydrogen Evolution Catalysis from Chemically Exfoliated Metallic MoS_2 Nanosheets. *J. Am. Chem. Soc.* **2013**, *135*, 10274–10277.
35. Xie, J.; Zhang, J.; Li, S.; Grote, F.; Zhang, X.; Zhang, H.; Wang, R.; Lei, Y.; Pan, B.; Xie, Y. Controllable Disorder Engineering in Oxygen-Incorporated MoS_2 Ultrathin Nanosheets for Efficient Hydrogen Evolution. *J. Am. Chem. Soc.* **2013**, *135*, 17881–17888.
36. Kibsgaard, J.; Chen, Z.; Reinecke, B. N.; Jaramillo, T. F. Engineering the Surface Structure of MoS_2 to Preferentially Expose Active Edge Sites for Electrocatalysis. *Nat. Mater.* **2012**, *11*, 963–969.
37. Yu, Y.; Huang, S.-Y.; Li, Y.; Steinmann, S. N.; Yang, W.; Cao, L. Layer-Dependent Electrocatalysis of MoS_2 for Hydrogen Evolution. *Nano Lett.* **2014**, *14*, 553–558.
38. Kong, D.; Wang, H.; Cha, J. J.; Pasta, M.; Koski, J. K.; Yao, J.; Cui, Y. Synthesis of MoS_2 and $MoSe_2$ Films with Vertically Aligned Layers. *Nano Lett.* **2013**, *13*, 1341–1347.
39. Tsai, C.; Abild-Pedersen, F.; Nørskov, J. K. Tuning the MoS_2 Edge-Site Activity for Hydrogen Evolution *via* Support Interactions. *Nano Lett.* **2014**, *14*, 1381–1387.
40. Jaramillo, T. F.; Jørgensen, K. P.; Bonde, J.; Nielsen, J.H.; Horch, S.; Chorkendorff, I. Identification of Active Edge Sites for Electrochemical H_2 Evolution from MoS_2 Nanocatalysts. *Science* **2007**, *317*, 100–102.
41. Zhao, Y.; Luo, X.; Li, H.; Zhang, J.; Araujo, P. T.; Gan, C. K.; Wu, J.; Zhang, H.; Quek, S. Y.; Dresselhaus, M. S.; *et al.* Interlayer Breathing and Shear Modes in Few-Trilayer MoS_2 and WSe_2. *Nano Lett.* **2013**, *13*, 1007–1015.
42. Xiang, Q.; Yu, J.; Jaroniec, M. Synergetic Effect of MoS_2 and Graphene as Cocatalysts for Enhanced Photocatalytic H_2 Production Activity of TiO_2 Nanoparticles. *J. Am. Chem. Soc.* **2012**, *134*, 6575–6578.
43. Feng, J.; Qian, X.; Huang, C.-W.; Li, J. Strain-Engineered Artificial Atom as a Broad-Spectrum Solar Energy Funnel. *Nat. Photonics* **2012**, *6*, 866–872.
44. High, A. A.; Novitskaya, E. E.; Butov, L. V.; Hanson, M.; Gossard, A. C. Control of Exciton Fluxes in an Excitonic Integrated Circuit. *Science* **2008**, *321*, 229–231.
45. Sevik, C. Assessment on Lattice Thermal Properties of Two-dimensional Honeycomb Structures: Graphene, h-BN, h-MoS_2, and h-$MoSe_2$. *Phys. Rev. B* **2014**, *89*, 035422.
46. Berkdemir, A.; Gutiérrez, H. R.; Botello-Méndez, A. R.; Perea-López, N.; Elías, A. L.; Chia, C.-I; Wang, B.; Crespi, V. H.; López-Urías, F.; Charlier, J.-C.; *et al.* Identification of Individual and Few Layers of WS_2 Using Raman Spectroscopy. *Sci. Rep.* **2013**, *3*, 1755.
47. Li, H.; Zhang, Q.; Yap, C. C. R.; Tay, B. K.; Edwin, T. H. T.; Olivier, A.; Baillargeat, D. From Bulk to Monolayer MoS_2: Evolution of Raman Scattering. *Adv. Funct. Mater.* **2012**, *22*, 1385–1390.
48. Chakraborty, B.; Bera, A.; Muthu, D.; Bhowmick, S.; Waghmare, U.; Sood, A. Symmetry-Dependent Phonon Renormalization in Monolayer MoS_2 Transistor. *Phys. Rev. B* **2012**, *85*, 161403.
49. Rice, C.; Young, R.; Zan, R.; Bangert, U.; Wolverson, D.; Georgiou, T.; Jalil, R.; Novoselov, K. Raman-scattering Measurements and First-Principles Calculations of Strain-Induced Phonon Shifts in Monolayer MoS_2. *Phys. Rev. B* **2013**, *87*, 081307.
50. Tongay, S.; Zhou, J.; Ataca, C.; Liu, J.; Kang, J. S.; Matthews, T. S.; You, L.; Li, J.; Grossman, J.; Wu, J. Broad-range Modulation of Light Emission in Two-Dimensional Semiconductors by Molecular Physisorption Gating. *Nano Lett.* **2013**, *13*, 2831–2836.
51. Buscema, M.; Steele, G. A.; van der Zant, H. S.; Castellanos-Gomez, A. The Effect of the Substrate on the Raman and Photoluminescence Emission of Single-layer MoS_2. *Nano Res.* **2014**, *7*, 561–571.
52. Zhu, Z.; Cheng, Y.; Schwingenschlögl, U. Giant Spin-Orbit-Induced Spin Splitting in Two-Dimensional Transition-Metal Dichalcogenide Semiconductors. *Phys. Rev. B* **2011**, *84*, 153402.
53. Chen, W.; Santos, E. J.; Zhu, W.; Kaxiras, E.; Zhang, Z. Tuning the Electronic and Chemical Properties of Monolayer MoS_2 Adsorbed on Transition Metal Substrates. *Nano Lett.* **2013**, *13*, 509–514.
54. Conway, B.; Tilak, B. Interfacial Processes Involving Electrocatalytic Evolution and Oxidation of H_2, and the Role of Chemisorbed H. *Electrochim. Acta* **2002**, *7*, 3571–3594.